

## ELECTRONIC SUPPLEMENTARY INFORMATION (ESI)

### Localized Three-Photon Upconversion Enhancement in Silver Nanowire Networks and its Effect in Thermal Sensing

Eduardo D. Martínez,<sup>\*a,b,c</sup> Luiz H. A. R. Ferreira,<sup>d</sup> Albano N. Carneiro Neto,<sup>e</sup> Carlos D. Brites<sup>e</sup> and Luis D. Carlos<sup>e</sup>

#### 1 Materials

The following reagents were obtained from Sigma-Aldrich Co.: erbium(III) oxide (CAS 12061-16-4), ytterbium(III) oxide (CAS 1314-37-0), gadolinium(III) oxide (CAS 1314-37-0), oleic acid (OA, technical grade, 90%), 1-octadecene (ODE, technical grade, 90%), PVP (360 000 g mol<sup>-1</sup>), anhydrous ethylenglycol (EtGOH, 99.8%) and AgNO<sub>3</sub> (99.9999%). All commercial reagents were used as received without further purification. We prepared rare-earth acetates in our laboratory using the corresponding rare-earth oxides (X<sub>2</sub>O<sub>3</sub>, X = Yb, Gd, Er) as follows. In a 500 mL round-bottom flask, we added ~1 g of each oxide to 30 mL of a 50% (v/v) aqueous solution of acetic acid. The mixture was refluxed for 1-2 hours until the oxides completely dissolved, resulting in a clear solution. Subsequently, we transferred the solution to a Pyrex open vessel and maintained it at 60 °C to allow the acid to evaporate. This process yielded the dried precipitates of acetate salts, which were then extracted.

#### 2 Synthesis of UCNPs

The synthesis of UCNPs followed the coprecipitation route adapted from Wang et al<sup>1</sup> and Li et al<sup>2</sup>. In a 250 mL round-bottom flask, we added 15 mL of ODE and 6 mL of OA. Then, 3.9 mL of a 0.2 M stock solution of Y(COOCH<sub>3</sub>)<sub>3</sub>, 1 mL of a 0.2 M stock solution of Yb(COOCH<sub>3</sub>)<sub>3</sub> and 0.1 mL of a 0.2 M stock solution of Er(COOCH<sub>3</sub>)<sub>3</sub> were added to the reactor. The nominal molar ratio was 1:0.78:0.2:0.02 Na:Y:Yb:Er. The mixture was heated to 110 °C for 1 hour to dissolve the precursors and evaporate the water, followed by cooling to room temperature. Next, a freshly prepared mixture containing 2.5 mL of a 1 M NaOH methanol solution and 10.1 mL of 0.4 M NH<sub>4</sub>F solution in methanol was rapidly injected. The flask was then heated to 50 °C for 30 min and sealed. The temperature was further raised to 100 °C, and a vacuum pump was connected. After 15 min, the vacuum pump was turned off, a condenser was mounted, and the temperature was increased to 310 °C under an argon flux. After 90 min, the flask was removed from the mantle and allowed to cool to room temperature. The UCNPs were extracted by adding excess anhydrous ethanol and performing centrifugation in 15 mL conical tubes. Centrifugation was conducted at 1004 RCF (2400 rpm) for approximately 7 min. The precipitated UCNPs were then redispersed in 4 mL of cyclohexane, and ethanol was added to complete the volume. The centrifugation and washing procedure were repeated twice, and finally, the UCNPs were dispersed in 12 mL of cyclohexane.

<sup>a</sup> Gerencia Física, Centro Atómico Bariloche, Comisión Nacional de Energía Atómica (CNEA), Av. Bustillo 9500, S. C. de Bariloche (8400), Río Negro, Argentina. \*Tel: +54 0294 444 5900; E-mail: eduardo.martinez@cab.cnea.gov.ar

<sup>b</sup> Consejo Nacional de Investigaciones Científicas y Técnicas (CONICET), CCT Patagonia Norte, Av. de los Pioneros 2350, S. C. de Bariloche (8400), Río Negro, Argentina

<sup>c</sup> Instituto de Nanociencia y Nanotecnología (CNEA-CONICET), Av. Bustillo 9500, S. C. de Bariloche (8400), Río Negro, Argentina.

<sup>d</sup> "Gleb Wataghin" Institute of Physics, University of Campinas, UNICAMP 13083-859, Campinas, SP, Brazil.

<sup>e</sup> Phantom-g, CICECO, Departamento de Física, Universidade de Aveiro, Campus Santiago, Aveiro 3810-193, Portugal.

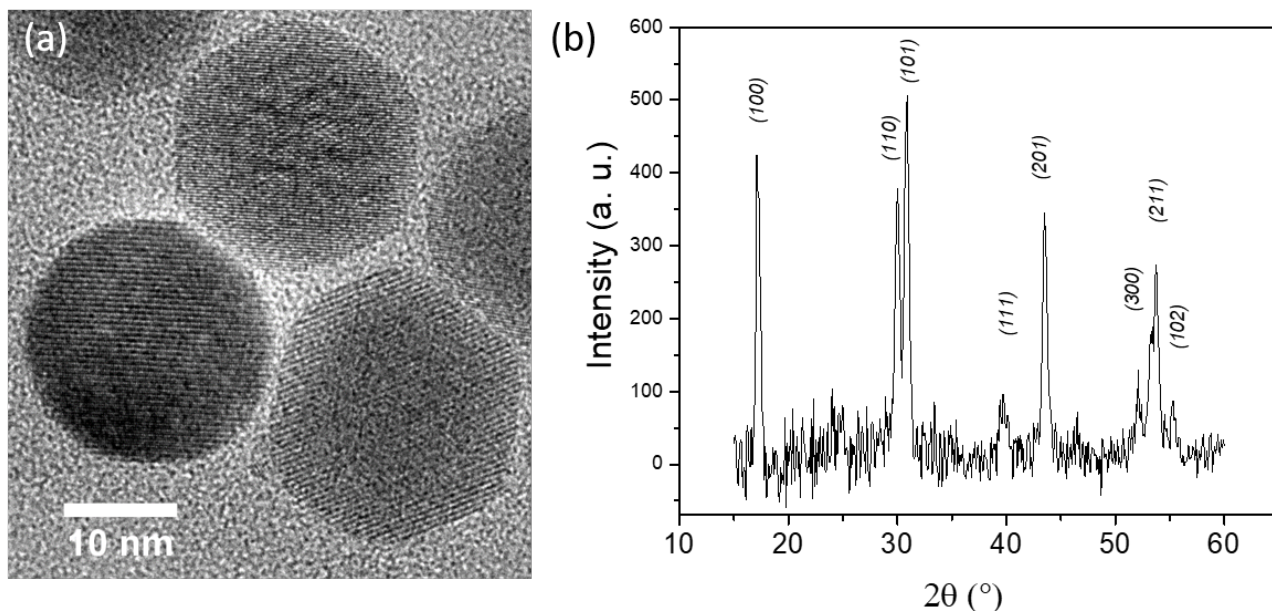


Fig. S1 (a) High-resolution TEM image and (b) X-ray Diffraction (XRD) data of the UCNPs utilized in this study, revealing all peaks corresponding to  $\beta$ - $\text{NaYF}_4$ . XRD analysis was conducted using a Bruker D2 Phaser instrument.

### 3 Synthesis of AgNWs

We followed a classical polyol method as described by Jiu et al.<sup>3</sup> Typically, 0.2 g of PVP ( $360000 \text{ g mol}^{-1}$ ) were added to 25 mL of anhydrous ethylenglycol (EtGOH, 99.8%, Sigma-Aldrich) and dissolved at  $60^\circ\text{C}$ . After complete dissolution and cooling to room temperature, 0.25 g of  $\text{AgNO}_3$  (99.9999% Sigma-Aldrich) were added and dissolved in darkness under strong stirring. Then, 3.25 g of a  $0.6 \mu\text{M}$   $\text{FeCl}_3$  solution in EtGOH were added and the mixture was stirred for 1 min. The mixture was quickly transferred to a 100 mL Schott type flask, sealed, and placed in a pre-heated oven at  $130^\circ\text{C}$  for 5 h. The AgNWs were washed and extracted using mixtures of acetone and isopropanol (IPA) and multiple cycles of centrifugation. AgNWs were finally dispersed in IPA as stock solutions. To achieve a homogeneous distribution of the AgNWs upon deposition, an aqueous colloid was formulated with the addition of a 2 wt% PSS solution in the following proportion: AgNWs-IPA:PSS: $\text{H}_2\text{O}$  4.5:0.5:10. The fraction of coverage of the surface was obtained using dark-field optical microscopy images as the ratio between the surface area covered by the AgNWs and the total surface area.

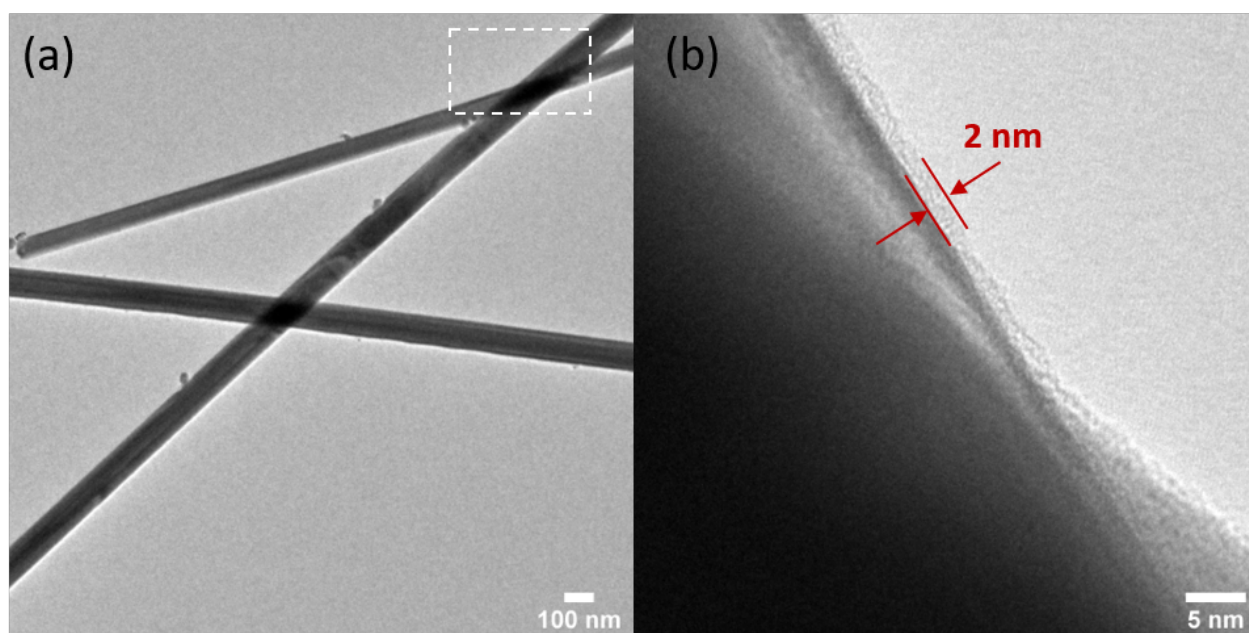


Fig. S2 (a, b) Transmission Electron Microscopy (TEM) images of AgNWs. In (b), a layer of polyvinylpyrrolidone (PVP) approximately 2 nm thick envelops the AgNWs.

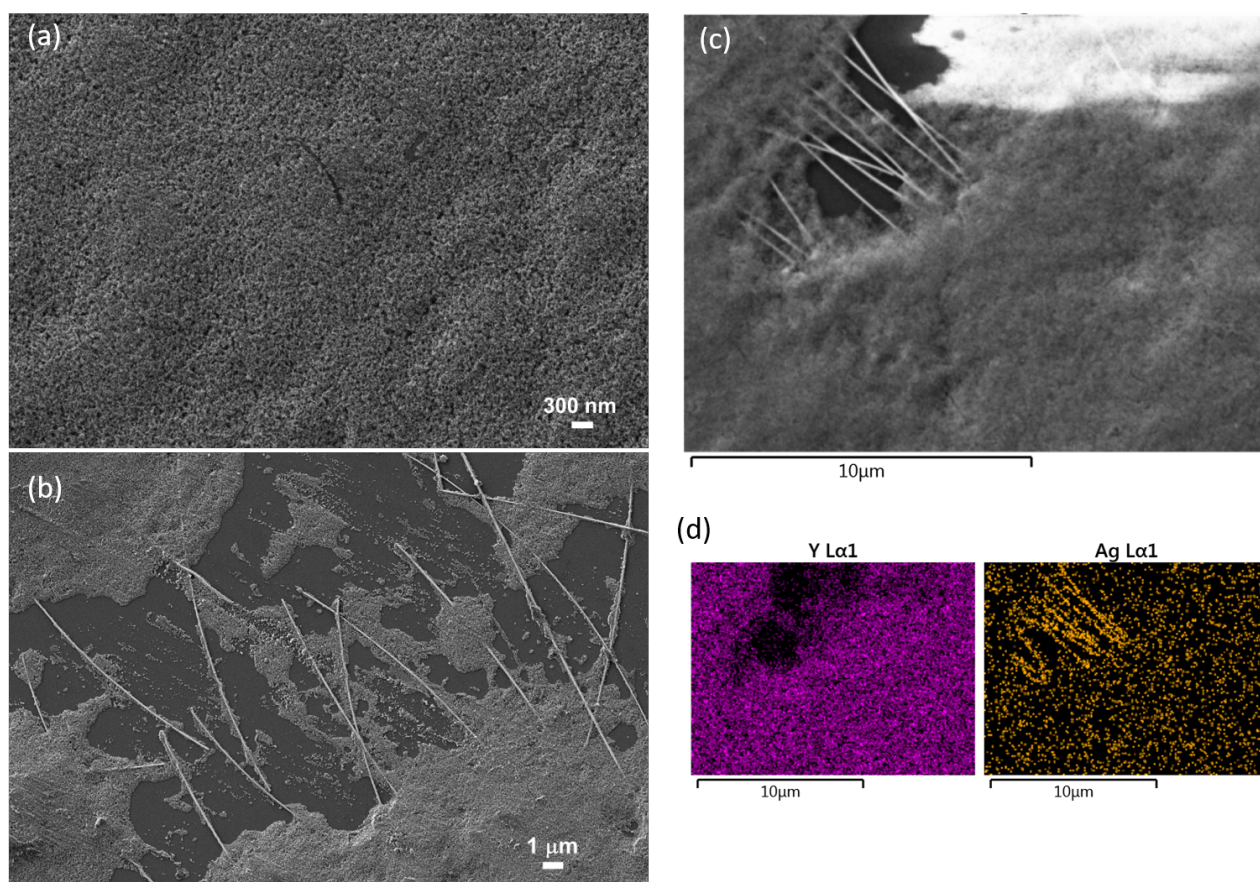


Fig. S3 Additional images depicting the deposition of UCNPs onto AgNW networks. Various regions display non-uniform coverage of UCNPs. (a) A fully covered region, (b) absence of specific accumulation at NW junctions, (c,d) Energy Dispersive X-ray Spectroscopy (EDS) imaging revealing the spatial distribution of silver (Ag) in AgNWs and yttrium (Y) in UCNPs.

#### 4 Calibration of UCNPs thermometers

A cover slide with a thin deposit of the UCNPs made by drop-casting was placed on a heating film made up of a silver nanowire network.<sup>4</sup> A reference thermometer (either an RTD Pt100 or a thermistor) were placed on top of the cover slide with a thermal grease HY710 for improving the thermal contact. A temperature controller Novus N321-Pt100 was used to set the temperature to a fixed value with a precision of  $\pm 0.2$  K for temperature below 320 K and  $\pm 0.5$  K for higher temperatures. Emission spectra were acquired using a 980 nm diode laser with nominal power of 20.28 mW under non-focused conditions to minimize the presence of the H9/2 band. Five consecutive spectra with 2 s acquisition time were obtained at controlled temperatures and averaged. Calculation of the thermometric parameter ( $\Delta$ ) was done by full or partial integration methods. We integrate the  $I_H$  band spectra between 500 nm and 535.5 nm while the  $I_S$  band was calculated by integration from 535.5 nm and 570 nm for the full integration and from 535.5 nm and 555.5 nm for the partial integration method. We plot the obtained data in a linearized according to the Boltzmann model. From the slope of a linear regression we calculated the energy difference ( $\Delta E$  ( $\text{cm}^{-1}$ )) between levels  $^4S_{3/2}$  and  $^2H_{11/2}$ . The relative sensitivity was also obtained at each temperature. Results of the calibration procedure are shown in Figure S4.

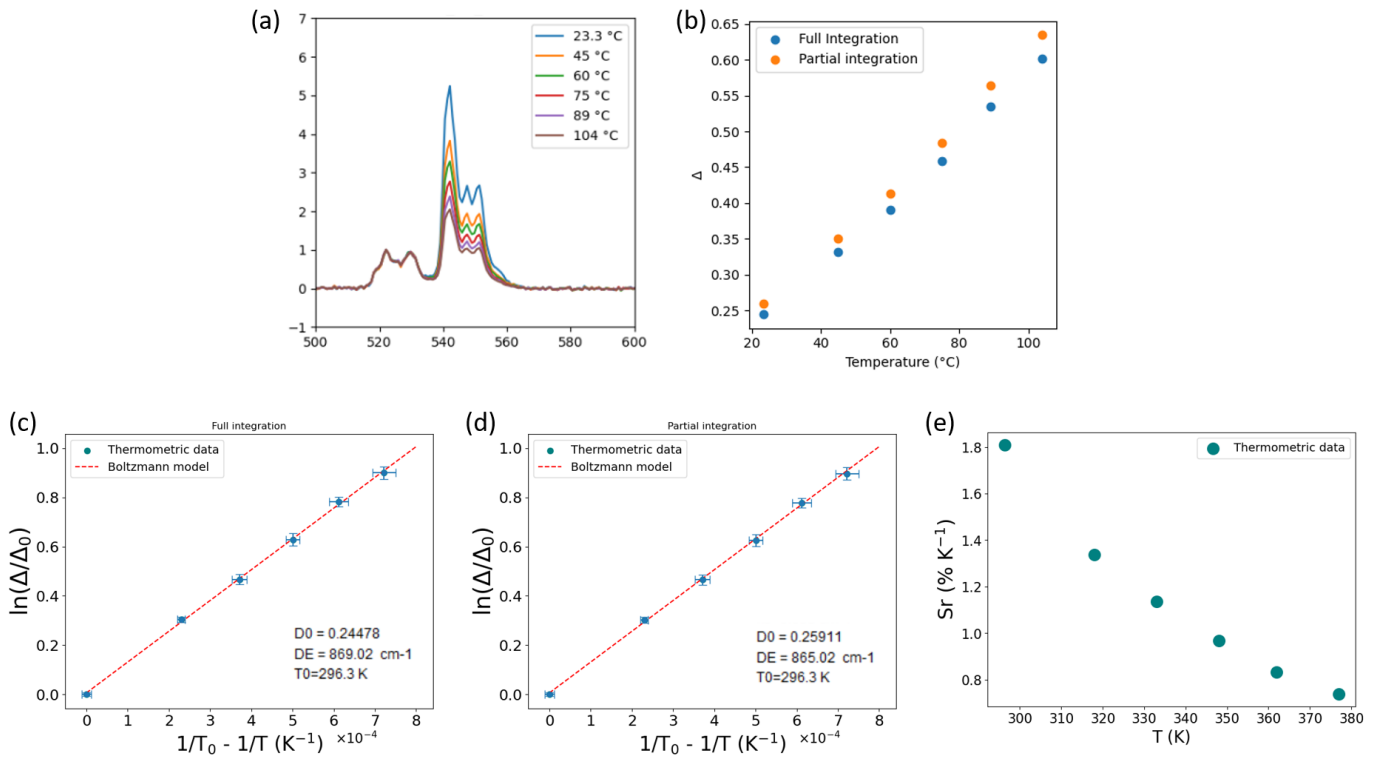


Fig. S4 Calibration data obtained for UCNPs. (a) Emission spectra at increasing temperatures. (b,d) Linearized thermometric data and fitting using the Boltzmann model. (e) Relative sensitivity of UCNPs at varying temperatures measured in out-of focus conditions.

The analysis of HSM images and the calculation of the thermometric parameter on spectra collected on each pixel, a baseline correction algorithm was applied to the raw data. Spectral data apart from the emission lines were used to fit a linear function that was then subtracted to the raw spectra.

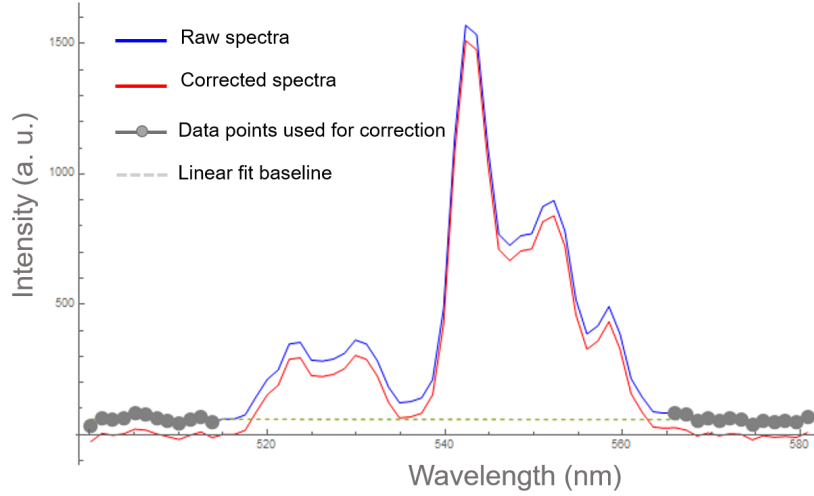


Fig. S5 Baseline correction method performed on spectra at each pixel. A linear fit using points marked in gray dots is substrated to the spectra. The resulting corrected spectra (in red) were utilized for thermometric analysis.

Table S1 Data obtained from emission spectra on selected points of interest of Fig. 2 (main text).

	P1	P2	P3	P4	P5	P6	P7	P8
Total Intensity ( $I_{Total}$ )	120606	7160	228371	3487	53470	846	20246	998
Intensity H9/2 ( $I_{H9/2}$ )	16392	648	41625	308	6756	92	2378	84
$I_{H9/2}/I_{Total}$	0.1359	0.0905	0.1822	0.0883	0.1263	0.1092	0.1175	0.0841
Delta (FI)	0.2146	0.2407	0.1895	0.2465	0.2172	—	0.2348	—
Delta (PI)	0.2570	0.2712	0.2419	0.2770	0.2566	—	0.2747	—
Temperature (FI) (K)	287.3	295.1	279.3	296.8	288.1	—	293.4	—
Temperature (PI) (K)	295.7	299.5	291.5	301.1	295.6	—	300.5	—

Procedure performed on a particular spectra is shown as an example in Figure S5.

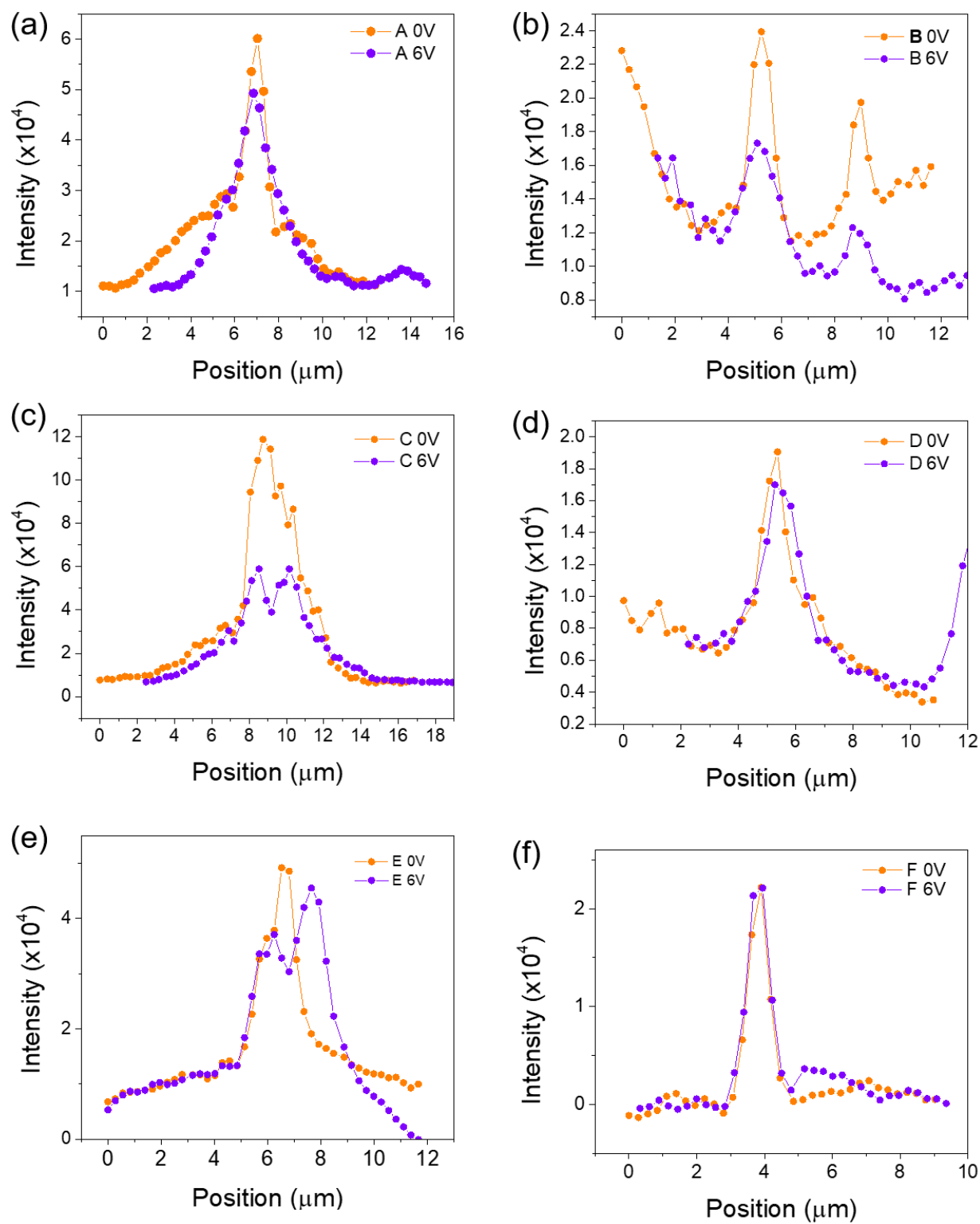


Fig. S6 (a-f) Total intensity profile across lines A-E (Fig. 3, main text) measured under 0 V and 6 V of applied voltage.

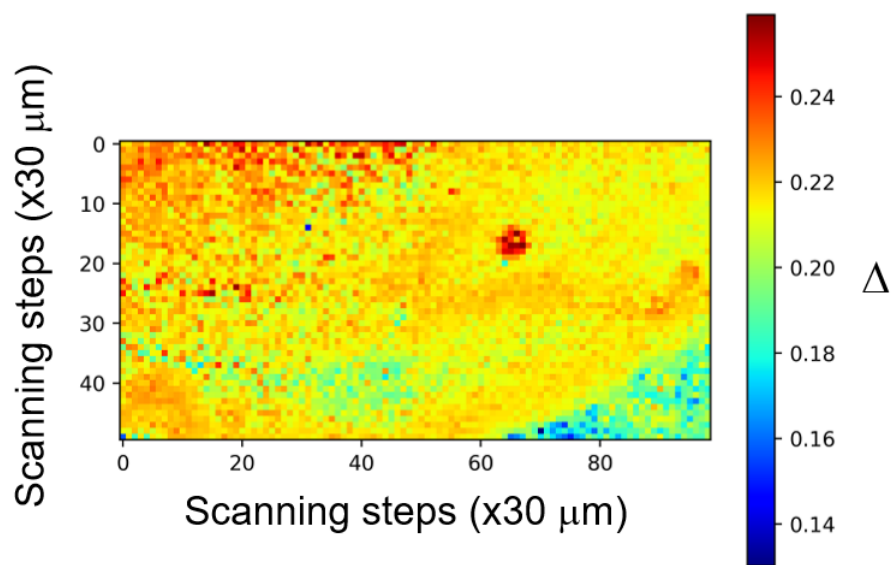


Fig. S7 Thermometric map of a glass sample with a deposit of AgNWs on half of its surface (right side) obtained by scanning luminescence thermometry.  $\Delta$  values were calculated using the full-integration method from 534 nm to 570 nm. Thermometric parameters on the right side (w/AgNWs) are slightly lower than the ones obtained without AgNWs (left side).

## 5 Calculation of the signal-to-noise ratio (SNR)

The SNR on each pixel was calculated as follows.<sup>5</sup> The experimentally detected signal intensity ( $s$ ) can be physically described, in a linear approximation, as the product of the detector gain ( $\alpha$ ), the quantum yield ( $Q$ ) of the photon-to-electron conversion in the detector, and the number ( $N$ ) of incoming photons, as:  $s = \alpha QN$ . On the other hand, the dark noise ( $\sigma_{dark}$ ) is expressed as  $\sigma_{dark} = \alpha\beta(T)t$  where  $\beta$  is a thermal factor dependent on the temperature of the detector and  $t$  is the acquisition time. Experimentally, we can evaluate  $\sigma^{dark}$  at a given pixel, indexed as  $i, j$ , by calculating the square differences between data points at successive wavelengths (index  $k$ ) in the off-emission region as stated below:

$$\sigma_{ij}^{dark} = \frac{B^{total}}{B^{off}} \sqrt{\sum_{k=1}^{B^{off}} (I_{ij}(\lambda_{k+1}) - I_{ij}(\lambda_k))^2} \quad (S1)$$

where  $B^{total}$  is the total number of spectral points in the spectrum (66 bands) and  $B^{off}$  is the number of wavelengths in the off-emission region (25 bands). In addition, considering the intensity detected as proportional to the number of collected photons, we can calculate the shot noise as proportional to the square root of the measured intensity:

$$\sigma^{shot} = \alpha \sqrt{QN} \propto \sqrt{I}. \quad (S2)$$

Therefore, the total noise is given by:

$$\sigma^{total} = \sqrt{(\sigma^{dark})^2 + (\sigma^{shot})^2}. \quad (S3)$$

With these components, it is possible to quantify the signal-to-noise ratio (SNR) at any  $i, j$  pixel of the hyperspectral image as:

$$SNR_{ij} = \frac{\alpha QN}{\sqrt{(\sigma^{dark})^2 + (\sigma^{shot})^2}} \sim \frac{I_{ij}}{\sqrt{(\sigma_{ij}^{dark})^2 + I_{ij}}}. \quad (S4)$$

## 6 Calculation of the enhancement factor and the energy transfer rates

The radiative rate from an emitting state  $\psi J$ , involving the  $\psi J \rightarrow \psi' J'$  transition can be calculated using the following equations:

$$A_{rad} = \frac{4e^2\omega^3}{3\hbar c^3(2J+1)} [\chi S_{ed} + n_r^3 S_{md}] \quad (S5)$$

where  $e$  is the elementary charge,  $\omega$  is the angular frequency of the transition,  $\hbar$  is the reduced Planck's constant,  $c$  is the speed of light,  $\chi = n_r(n_r^2 + 2)^2/9$  is the Lorentz local field correction with  $n_r$  being the index of refraction of the medium. The quantities  $S_{ed}$  and  $S_{md}$  represent the electric and magnetic dipole strengths of the  $\psi J \rightarrow \psi' J'$  transition and can be calculated as:

$$S_{ed} = e^2 \left( \sum_{\lambda=2,4,6} \Omega_\lambda \cdot \left| \langle \psi J \| U^{(\lambda)} \| \psi' J' \rangle \right|^2 \right) \quad (S6)$$

$$S_{md} = \mu_B^2 \left| \langle \psi J \| L + 2S \| \psi' J' \rangle \right|^2. \quad (S7)$$

From the electric dipole strength perspective (Eq. S6),  $\Omega_\lambda$  ( $\lambda = 2, 4$ , and  $6$ ) represent the Judd-Ofelt intensity parameters, while  $\langle \psi J \| U^{(\lambda)} \| \psi' J' \rangle$  denotes the reduced matrix elements of the tensor operator of rank  $\lambda$ . Specifically for the  $\text{Yb}^{3+} {}^2F_{7/2} \rightarrow {}^2F_{5/2}$  transition, the values of  $\left| \langle {}^2F_{5/2} \| U^{(\lambda)} \| {}^2F_{7/2} \rangle \right|^2$  are 0.1225, 0.4096, and 0.8575 for  $\lambda = 2, 4$ , and  $6$ , respectively.<sup>6</sup> Moving to the magnetic dipole strength side (Eq. S7),  $\mu_B$  represents the Bohr magneton  $\mu_B = e\hbar/(2m_e c)$  (with  $m_e$  being the electron mass) and  $\langle \psi J \| L + 2S \| \psi' J' \rangle$  are the reduced matrix elements of orbital and spin angular momentum operators ( $L$  and  $S$ ). The value of  $\left| \langle {}^2F_{5/2} \| L + 2S \| {}^2F_{7/2} \rangle \right|^2 = 2.5719$  was calculated elsewhere.<sup>7</sup> The selection rules for these transitions are as follows:  $|J - J'| \leq \lambda \leq J + J'$  for  $S_{ed}$  and  $|J - J'| = 0, 1$  (with the exception of  $J = J' = 0$ ) for  $S_{md}$ . The oscillator strength is given by:

$$f_{osc} = \frac{(2J+1)}{(2J-1)} \frac{m_e c^3}{2e^2 \omega^2 n_r^2} A_{rad}. \quad (S8)$$

Utilizing the relationship between the spontaneous emission coefficient and the oscillator strength of a transition outlined above, it is straightforward to express it in terms of  $S_{ed}$  and  $S_{md}$ . Thus, the oscillator strength  $f_{osc}$  can be calculated as follows:

$$f_{osc} = \frac{2\omega m_e}{3\hbar(2J'+1)e^2} \left[ \frac{(n_r^2 + 2)^2}{9n} S_{ed} + n_r S_{md} \right]. \quad (S9)$$

The limitations of the Judd-Ofelt analysis arise when applied to  $\text{Yb}^{3+}$  due to its sole excited 4f state. Consequently, it is not possible to construct a set of three equations with three parameters to be determined experimentally using the least-squares method.<sup>8</sup> Put simply, determining Judd-Ofelt parameters for  $\text{Yb}^{3+}$  can result in multiple solutions and mathematical ambiguity. Thus, assuming the values of  $\Omega_\lambda$  (in units of  $\text{cm}^2$ ) for  $\text{Yb}^{3+}$  in  $\text{NaYF}_4:\text{Yb}^{3+}$ :  $\Omega_2 = 1.62 \times 10^{-20}$ ,  $\Omega_4 = 1.07 \times 10^{-20}$ , and  $\Omega_6 = 1.59 \times 10^{-20}$ , we obtain:

$$\sum_{\lambda=2,4,6} \Omega_{\lambda} \left| \left\langle {}^2F_{5/2} \left\| U^{(\lambda)} \right\| {}^2F_{7/2} \right\rangle \right|^2 = 2.00 \times 10^{-20} \text{cm}^2 \quad (\text{S10})$$

which agrees with Kushida's estimations.<sup>6</sup> Now, with (index of refraction for  $\beta$ -NaYF<sub>4</sub> matrix,<sup>9</sup>)  $\omega = 1.92 \times 10^{15} \text{s}^{-1}$  ( $\sim 980 \text{ nm}$ ), and applying the value above leads to:

$$f_{osc} = 3.82 \times 10^{-6}. \quad (\text{S11})$$

This falls within the typical range of oscillator strengths for the  $\text{Yb}^{3+} {}^2F_{7/2} \rightarrow {}^2F_{5/2}$  transition.<sup>6,8,10,11</sup>

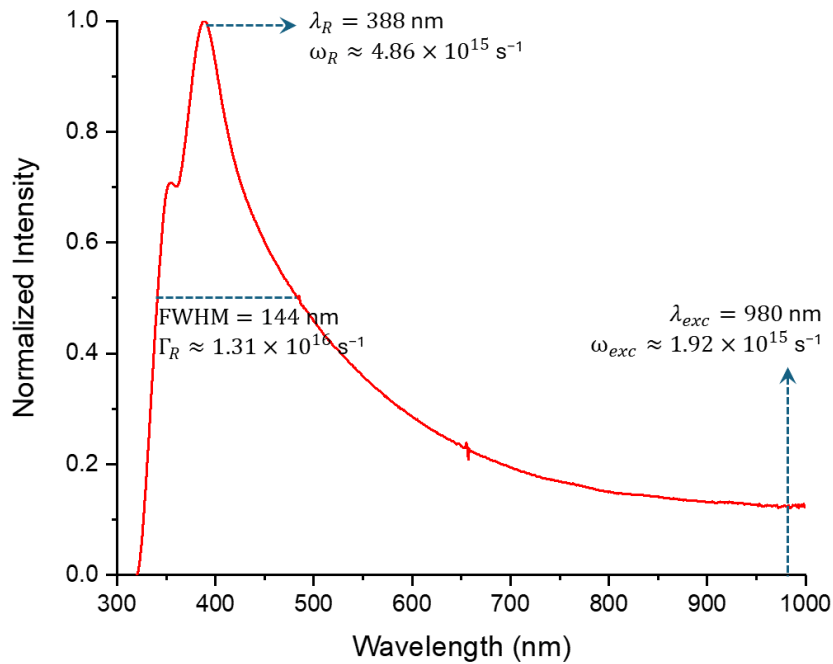


Fig. S8 UV-Visible spectra of an isopropanol colloid containing AgNWs. Frequency-dependent parameters of the silver nanowire used in Eq. S8 are indicated.

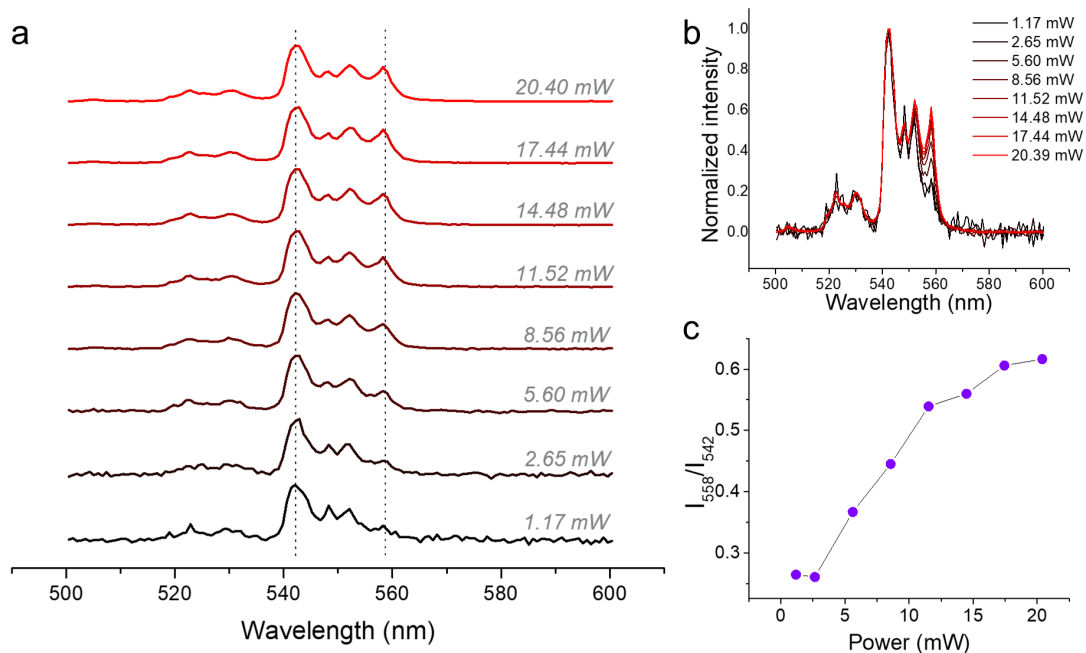


Fig. S9 Effect of the excitation intensity on the emission spectra. a) Normalized emission spectra of UCNP under excitation of a 980 nm laser light at increasing power. Light was focused on a spot size of  $16\mu\text{m}^2$  using a 10X objective lens. b) Comparison of normalized spectra at increasing excitation power. c) Ratio of the intensity at 558 nm ( ${}^2\text{H}_{9/2} \rightarrow {}^4\text{I}_{13/2}$ ) vs. intensity at 542 nm ( ${}^4\text{S}_{3/2} \rightarrow {}^4\text{I}_{15/2}$ ) as a function of the power of the excitation light.

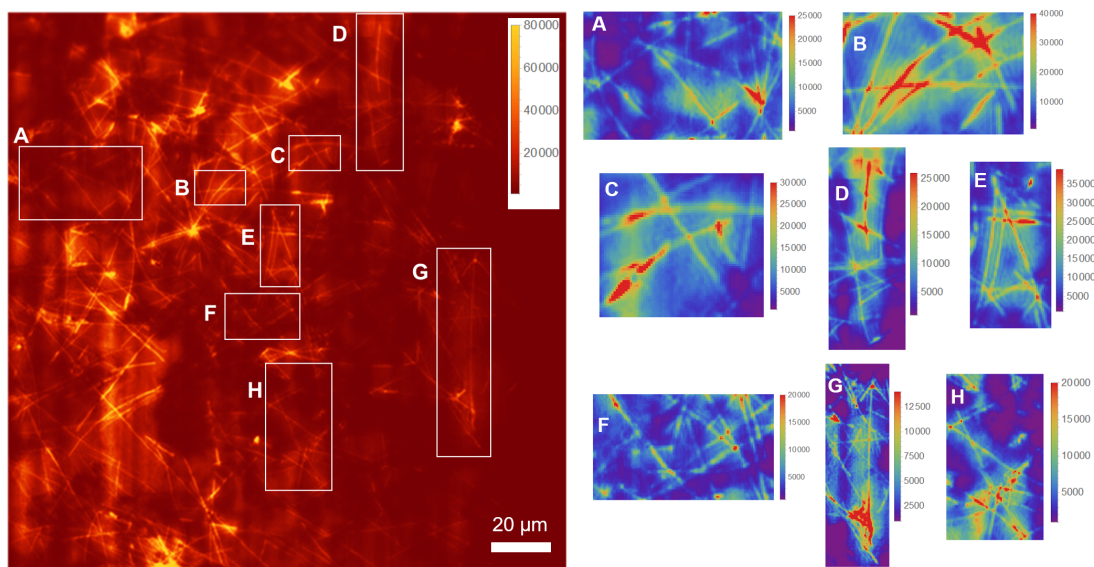


Fig. S10 Close up analysis of the intensity map showing the local enhancement at junctions of AgNWs in different regions of the HSM image.

## Notes and references

- 1 F. Wang, R. Deng and X. Liu, *Nature Protocols*, 2014, **9**, 1634–1644.
- 2 D. Li, Q. Shao, Y. Dong and J. Jiang, *Journal of Rare Earths*, 2014, **32**, 1032–1036.
- 3 J. Jiu, T. Araki, J. Wang, M. Nogi, T. Sugahara, S. Nagao, H. Koga, K. Suganuma, E. Nakazawa, M. Hara, H. Uchida and K. Shinozaki, *Journal of Materials Chemistry A*, 2014, **2**, 6326–6330.
- 4 E. D. Martínez, A. F. García Flores, H. Pastoriza, R. R. Urbano and C. Rettori, *Sensors and Actuators B: Chemical*, 2018, **259**, 475–483.
- 5 E. D. Martínez, C. D. Brites, R. R. Urbano, C. Rettori and L. D. Carlos, *Physica B: Condensed Matter*, 2022, **629**, 413639.
- 6 T. Kushida, *Journal of the Physical Society of Japan*, 1973, **34**, 1318–1326.
- 7 M. Oggianu, V. Marneli, M. A. Hernández-Rodríguez, N. Monni, M. Souto, C. D. Brites, C. Cannas, F. Manna, F. Quochi, E. Cadoni, N. Masciocchi, A. N. Carneiro Neto, L. D. Carlos and M. L. Mercuri, *Chemistry of Materials*, 2024, **36**, 3452–3463.
- 8 W. T. Carnall, P. R. Fields and B. G. Wybourne, *The Journal of Chemical Physics*, 1965, **42**, 3797–3806.
- 9 V. I. Sokolov, A. V. Zvyagin, S. M. Igumnov, S. I. Molchanova, M. M. Nazarov, A. V. Nechaev, A. G. Savelyev, A. A. Tyutyunov, E. V. Khaydukov and V. Y. Panchenko, *Optics and Spectroscopy*, 2015, **118**, 609–613.
- 10 O. Malta, *Journal of Non-Crystalline Solids*, 2008, **354**, 4770–4776.
- 11 J. Dexpert-Ghys and F. Auzel, *The Journal of Chemical Physics*, 1984, **80**, 4003–4012.
- 12 A. M. Aguilar, E. L. Saidman, M. V. Rosato-Siri, L. Marpegán and E. D. Martínez, *ACS Applied Nano Materials*, 2023, **6**, 20942–20953.